Check for updates

Investigation on heterogeneous Rh catalysts for the hydroformylation of 1,3-butadiene to adipic aldehyde†

Lijin Gan, Zekun Liu, Lei Feng, Yi Duan, Guangyuan Xu, Si Chen and Huan Yan [iD] *

Adipic aldehyde, a precursor for polymers, has significant industrial applications, where the hydroformylation of 1,3-butadiene is a promising route to fabricate adipic aldehyde. However, the heterogeneous hydroformylation of 1,3-butadiene has been rarely reported. In this work, we reported ligand-modified Rh-supported single-atom catalysts and investigated them for efficient hydroformylation of 1,3-butadiene. Among the selected phosphine ligand candidates, the L11 ligand (NiXantphos) coordinated Rh atoms could achieve the highest selectivity to adipic aldehyde. Furthermore, *in situ* CO DRIFTS indicated that active species similar to homogeneous catalysts were formed on the surface of the ligand modified and supported Rh catalyst during the reaction, demonstrating the similar hydroformylation mechanism and origins of the various products.

Introduction

The atom-economical hydroformylation is a vital chemical process in the industrial transformation, providing aldehydes as important platform molecules for various industrial processes.[1,2] As a promising chemical intermediate to valued C_6 chemicals (1,6-hexanedioic acid, 1,6-hexanediol, and 1,6-hexanediamine) for polymer synthesis, 1,6-hexanedial (adipic aldehyde) has attracted widespread attention among all the aldehydes. Adipic aldehyde could be fabricated *via* the hydroformylation of 1,3-butadiene. As reported in the literature, the reaction of 1,3-butadiene to adipic aldehyde is currently catalyzed by homogeneous Rh–P complexes.[3–8] Homogeneous catalysts have high reactivity, but they suffer from difficulty and high cost in separation and recycling.[9]

Given the above issues, considerable efforts have been devoted to the development of heterogeneous hydroformylation. Heterogeneous catalytic designs for the hydroformylation of monoalkenes to aldehydes have been reported. The catalytic designs can be categorized into three types: immobilization of homogeneous complexes onto supports,[10–13] ligand modification of Rh nanoparticles,[14–17] and single-atom catalysts.[18–29] Grafting complexes onto supports is a straightforward method for the heterogenization of

homogeneous catalysts. Meijboom *et al.*[12] anchored Rh(I) complexes onto mesoporous MCM-41 and SBA-15 frameworks, obtaining immobilized catalysts *via* electrostatic methods. Employing these catalysts in the hydroformylation of 1-octene offered regioselectivity towards *n*-nonanal comparable to their homogeneous counterparts. The key to the regulation of hydroformylation activity and selectivity lies in ligands, so modification of ligands can also improve the hydroformylation activity and selectivity for heterogeneous Rh nanoparticle catalysts. Bell *et al.*[17] compared the activity and regioselectivity of ligand-modified Rh nanoparticle catalysts such as PPh₃–Rh/SiO₂ and Xantphos–Rh/SiO₂ in the hydroformylation of propylene, revealing that the Rh/SiO₂ catalyst modified with bidentate ligand Xantphos exhibited significantly enhanced activity and linear aldehyde selectivity. Compared to nanoparticle catalysts, single-atom catalysts have attracted significant attention due to their mononuclear structure similar to their homogeneous counterparts.[30] Copolymer-supported Rh catalysts with integrated phosphine ligands exhibited exceptional regioselectivity and activity in the process of alkene hydroformylation.[18–26] Compared with the multistep synthesis and high cost of polymer supports, inorganic oxide supports are more cost-effective and readily available. Ma and co-workers[28] constructed a highly active Rh/CeO₂ catalyst without ligands by tuning the coordination environment of Rh single atoms on CeO₂ *via* calcination temperature. In the hydroformylation reaction of propylene, the catalyst exhibited 100% selectivity for aldehydes without hydrogenation products propane and butanol. Addressing metal leaching and sintering in single-atom catalysts unmodified with ligands, Wang and co-workers[29] investigated the mechanism of Rh single-atom catalyst

Key Laboratory of Precision and Intelligent Chemistry, School of Chemistry and Materials Science, University of Science and Technology of China, Hefei, Anhui, 230026, P. R. China. E-mail: yanhuan1@ustc.edu.cn

aggregation and leaching, and greatly improved the stability of the catalyst by increasing the concentration of alkene. Considerable beneficial endeavors have been undertaken by previous researchers concerning the heterogeneous hydroformylation of monoalkenes. However, for the hydroformylation of diene (especially 1,3-butadiene), the heterogeneous catalyst design is still rarely reported.

In this work, we synthesized g-C_3N_4 supported Rh atoms with precise coordination engineering by various phosphine ligands. Atomic resolution HAADF-STEM confirmed the atomic dispersion of these as-prepared Rh catalysts, and the CO DRIFTS, ^{31}P MAS NMR, and XPS results further suggested the existence of the interaction between Rh atoms and electron-donating phosphine ligands. With this heterogeneous catalytic design, the Rh atoms could not only maintain the high hydroformylation activity with the largest dispersion but also demonstrate considerable potential for recycling. In these supported Rh catalysts, the electronic state and steric hindrance could be manipulated by the introduction of different phosphine ligands. Among 20 selected ligands, we found that Rh atoms could achieve the highest selectivity to adipic aldehyde with the employment of the NiXantphos (L11) ligand. Furthermore, *in situ* CO DRIFTS experimental results suggested that the formation of active species was similar to homogeneous catalysts under reaction conditions, indicating that the reaction mechanism of the hydroformylation process may be similar to the homogeneous counterpart.

Experimental

Materials

Synthesis gas (H_2 50%, CO 50%) with a purity of 99.999% was purchased from Dalian Special Gases Co., Ltd (Dalian, China). 1,3-Butadiene stock solution was prepared by bubbling 1,3-butadiene into toluene. The stock solution was stored at −30 °C and the concentration of 1,3-butadiene was periodically monitored by GC–MS. Adipic aldehyde (98%), cyclopentanecarbaldehyde (98%), 1-cyclopenten-1-carbaldehyde (98%), 4-pentenal (98%), 3-pentenal (98%), 2-pentenal (98%), valeraldehyde (98%) and 2-methylbutyraldehyde (98%) were purchased from Macklin Biochemical Co., Ltd (Shanghai, China). *n*-Nonane (99%), the internal standard for GC–MS analysis, was obtained from Aladdin Biochemical Technology Co., Ltd (Shanghai, China). $RhCl_3·3H_2O$ (≥98%) was purchased from ADAMAS-BETA (Shanghai, China). Urea (≥99%) was purchased from Sinopharm. Ligands (98%) were purchased from Aladdin Biochemical Technology Co., Ltd. (Shanghai, China). Toluene (≥99.5%) was used as the solvent for GC–MS analysis and was purchased from Sinopharm. All materials mentioned above were used without further purification.

Catalyst synthesis

Preparation of Rh/Al_2O_3 and ligand-modified Rh/Al_2O_3. Rh/Al_2O_3 was prepared by incipient wetness impregnation. $RhCl_3·3H_2O$ (51.2 mg, 0.19 mmol) was dissolved in 15 mL of deionized water, followed by the gradual addition of 2 g of nano Al_2O_3 with stirring. The resulting mixture was stirred at room temperature for 1 hour, then heated to 70 °C and stirred for another 8 hours. After cooling to room temperature, it was washed three times with an appropriate amount of deionized water. Upon completion of washing, the material was dried at 110 °C for 6 hours in a drying oven, followed by calcination at 300 °C for 3 hours with a heating rate of 5 °C min^{-1} using a tube furnace under an air atmosphere. After calcination, the sample $RhCl_3$/Al_2O_3 was treated with 10% hydrogen gas, initially held at room temperature for 30 minutes, then ramped to 300 °C at a rate of 5 °C min^{-1} and reduced for 2 hours to obtain Rh/Al_2O_3. The catalyst loading was determined through inductively coupled plasma optical emission spectroscopy (ICP-OES) testing. The modification of the ligand was carried out following standard Schlenk protocols. A requisite quantity of Rh/Al_2O_3 and a ligand denoted as L*n* ('*n*' represents the ligand number), equimolar to 20-fold the amount of Rh, were employed. Toluene was introduced in a suitable volume, and the mixture was subjected to reflux at 120 °C for 16 hours under an argon atmosphere. Upon cooling, it was repeatedly rinsed with hot toluene (70–80 °C) to remove physically adsorbed ligands, followed by vacuum drying at 80 °C for 24 hours, yielding L*n*–Rh/Al_2O_3.

Preparation of Rh/g-C_3N_4 and ligand-modified Rh/g-C_3N_4. g-C_3N_4 was prepared from urea according to the method described in the references.[31–33] In detail, 41.3 g of urea was weighed and placed in an alumina crucible, which was then covered and placed in a muffle furnace. The temperature was raised to 550 °C at a rate of 10 °C min^{-1} and maintained for 5 hours. A pale-yellow solid weighing 1.95 g was obtained, which was collected and used without further purification. The preparation of Rh/g-C_3N_4 was similar to that of Rh/Al_2O_3, except that the calcination atmosphere was argon. The preparation of L*n*–Rh/g-C_3N_4 followed the same procedure as L*n*–Rh/Al_2O_3.

Characterization

ICP-OES analysis was performed on an iCAP 7400 to determine the elemental percentage. X-ray diffraction (XRD) patterns were collected with a Rigaku TTR-III diffractometer with Cu Kα radiation at room temperature. The X-ray photoelectron spectra (XPS) were recorded on a Thermo ESCALAB250Xi spectrometer with an excitation source of monochromatized Al Kα (hv = 1486.6 eV) and a pass energy of 30 eV. The values of binding energies were calibrated with the C 1s peak of contaminant carbon at 284.80 eV. Aberration-corrected high-angle annular dark field scanning transmission electron microscopy (HAADF-STEM) was operated on a JEOL-F200 transmission electron microscope operating at 200 kV. *In situ* diffuse reflectance infrared Fourier transform spectroscopy (DRIFTS) measurements were performed on a Nicolet iS20 spectrometer equipped with a mercury–cadmium–telluride (MCT) detector and a high-temperature cell (Harrick) with ZnSe windows. The ^{31}P magic

angle spinning nuclear magnetic resonance (^{31}P MAS NMR) spectra were acquired using a 600 MHz WB solid-state nuclear magnetic resonance spectrometer.

Catalytic evaluation

In a typical hydroformylation experiment, appropriate quantities of 1,3-butadiene stock solution (with a butadiene quantity of 1 mmol), L11–Rh/g-C$_3$N$_4$ (with an Rh quantity of 0.01 mmol), 4 mL of toluene and a magnetic stirring bar were added into a 50 mL autoclave. The autoclave was sealed and purged with 2 MPa synthesis gas five times, and then pressurized with 4 MPa. Next, the autoclave was placed on a magnetic stirrer and heated to 90 °C for 10 hours. After completion, the reaction mixture was cooled to room temperature and the remaining gas was slowly released. Finally, the reaction mixture was diluted with toluene and subjected to qualitative and quantitative analysis using a gas chromatograph–mass spectrometer (GC–MS).

GC–MS was performed using a Shimadzu GCMS-QP2010 SE instrument with helium as the carrier gas. A capillary column SH-I-5Sil MS (30 m, 0.25 mm ID, 0.25 μm df) was used. The helium flow rate was maintained at 0.92 mL min^{-1}. The column temperature was initially held at 60 °C for 2 min and then increased at a rate of 10 °C min^{-1} to 200 °C, which was held for 5 min. The temperatures of both the vaporizer and the ion source were 200 °C. The retention times for selected products were as follows: 1,3-butadiene (1.55 min), 2-methyl butanal (2.14–2.15 min), 2-pentenal (2.89 min), 3-pentenal (2.36 min), 4-pentenal (2.26 min), n-pentanal (2.34 min), cyclopentanone (3.95–3.99 min), 1-cyclopentenone (4.66 min), and n-nonane (internal standard, 4.81 min). A representative GC–MS chromatogram is shown in the ESI† (Fig. S1). The conversion of 1,3-butadiene and the product selectivities were calculated according to the following formulae [eqn (1) and (2)]:

$$\text{Conversion (\%)} = \frac{n(\text{butadiene}) - n'(\text{butadiene})}{n(\text{butadiene})} \times 100 \quad (1)$$

$$\text{Selectivity (\%)} = \frac{n(\text{aldehydes formed})}{n(\text{total products})} \times 100 \quad (2)$$

where n(butadiene) = mol of 1,3-butadiene before the reaction and n'(butadiene) = mol of 1,3-butadiene after the reaction. The carbon balance for the hydroformylation of 1,3-butadiene was estimated according to the following formulae [eqn (3) and (4)]:

$$\text{Carbon balance (\%)} = \frac{n\text{C}(\text{aldehydes} + \text{butadiene})_{\text{product}}}{n\text{C}(\text{CO}) + n\text{C}(\text{butadiene})_{\text{feed}}} \times 100 \quad (3)$$

$$n\text{C}(\text{CO}) = [n(\text{syngas consumption from reservoir}) - n(\text{hydrogenation products})] \times 0.5 \quad (4)$$

Evidently, the C balance would be 100% for total selectivity to aldehydes. Any deviation from this was attributed to the formation of hydrogenation products and other by-products that were difficult to detect by GC–MS.

Results and discussion

Catalyst characterization

To avoid the acid sites from the support, a new neutral support, g-C$_3$N$_4$, was selected as the candidate for the following supported catalysts. As shown in Fig. 1a, RhCl$_3$·3H$_2$O was impregnated onto the g-C$_3$N$_4$ support, followed by reduction at 300 °C in an argon atmosphere. Subsequently, under standard Schlenk conditions, ligands were employed to modify the Rh single-atom catalyst (designated as Ln–Rh/g-C$_3$N$_4$, 'n' represents the ligand number). To determine the morphology of the as-prepared Rh catalysts, we resorted to HAADF-STEM. The images shown in Fig. 1b and d indicate that the Rh catalysts exhibit atomic dispersion without any obvious aggregation before and/or after ligand modification. For benchmark screening, a high loading of Rh catalyst (6.41 wt% of Rh/g-C$_3$N$_4$) was prepared. As XRD patterns shown in Fig. 1e, for Rh nanoparticles (Fig. S2†), Rh/g-C$_3$N$_4$ (6.41 wt%) with high Rh loading demonstrated classic peaks related to nanoparticles. In contrast, we observed that there were no classic XRD peaks for Rh nanoparticles in the Rh/g-C$_3$N$_4$ (1 wt%) catalysts, which was highly consistent with the STEM images.

To further shed light on the coordination between Rh atoms and phosphine ligands, CO adsorption DRIFTS and ^{31}P MAS NMR were performed over different phosphine ligand-modified Rh catalysts. The CO adsorption DRIFTS spectra of Rh/g-C$_3$N$_4$ and Ln–Rh/g-C$_3$N$_4$ modified with representative ligands are depicted in Fig. 2a. Rh/g-C$_3$N$_4$ exhibited two sharp bands at 2089 cm^{-1} and 2022 cm^{-1}, corresponding to Rh(CO)$_2$ species.[28,29] However, in the cases of Ln–Rh/g-C$_3$N$_4$ modified with phosphine ligands, the CO adsorption features vanished. This trend was possibly ascribed to the strong steric effect on Rh atoms derived from the coordinated phosphine ligands, thereby inhibiting the adsorption of CO. To further verify the coordination between the ligands and Rh atoms, ^{31}P MAS NMR was carried out on L11–Rh/g-C$_3$N$_4$ and control samples, as shown in Fig. 2b. The chemical shift of P in pure ligand L11 was observed at −19.4 ppm, while the chemical shift of P physically adsorbed on g-C$_3$N$_4$ was almost identical (−18.7 ppm), suggesting the negligible interaction with the support. However, for L11–Rh/g-C$_3$N$_4$, a new signal at 28 ppm was obvious and assigned to the P coordinated with Rh atoms.[16,17] Also, it gave the same scenario in other phosphine ligand coordinated catalysts (Fig. S4†). Taken together, the coordination between Rh atoms and the phosphine ligand indeed existed in all ligand-modified Rh catalysts. To investigate the electronic states of the Rh-related catalysts, XPS was performed for more detailed information. As demonstrated in Fig. 2c, for RhCl$_3$/g-C$_3$N$_4$ without reduction, the dominant surface species was Rh^{3+} (binding energy, BE = 309.6 eV). After the reduction of RhCl$_3$/g-C$_3$N$_4$, the surface Rh species were converted into Rh^{2+} species (BE = 309.0 eV). The binding energy shifted to a lower energy (308.8 eV) after phosphine ligand modification,
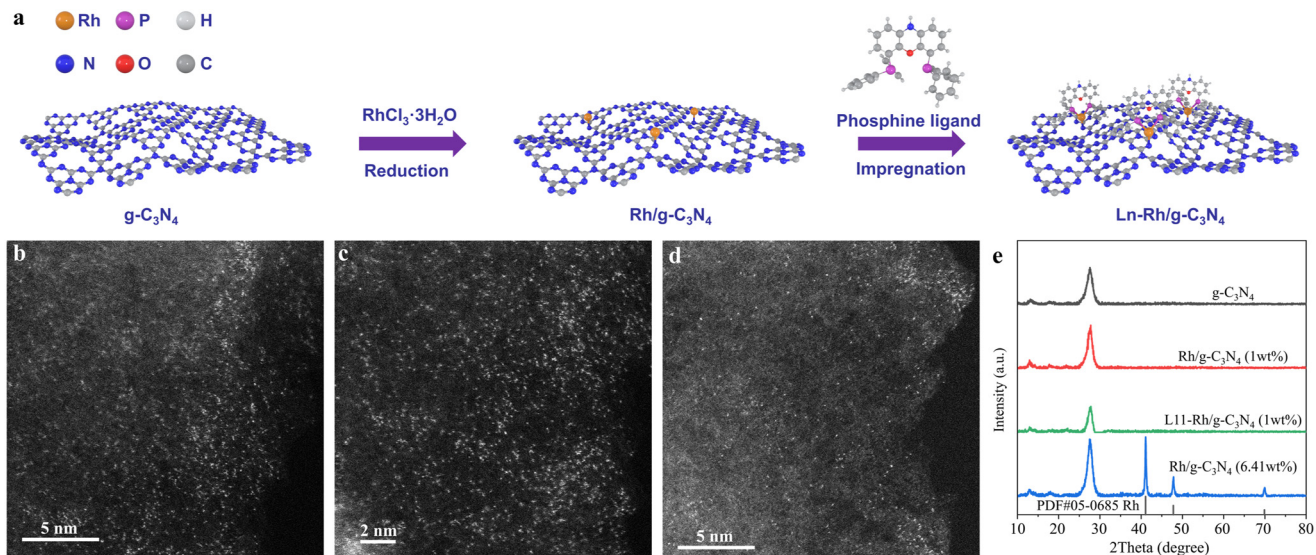
Fig. 1 (a) Schematic illustration of the synthesis of Rh/g-C_3N_4 and ligand-modified Rh/g-C_3N_4 catalysts. Representative HAADF-STEM images of (b) and (c) Rh/g-C_3N_4 (1 wt%) and (d) L11–Rh/g-C_3N_4 (1 wt%). (e) XRD patterns of g-C_3N_4, Rh/g-C_3N_4 (1 wt%), L11–Rh/g-C_3N_4 (1 wt%) and Rh/g-C_3N_4 (6.41 wt%).
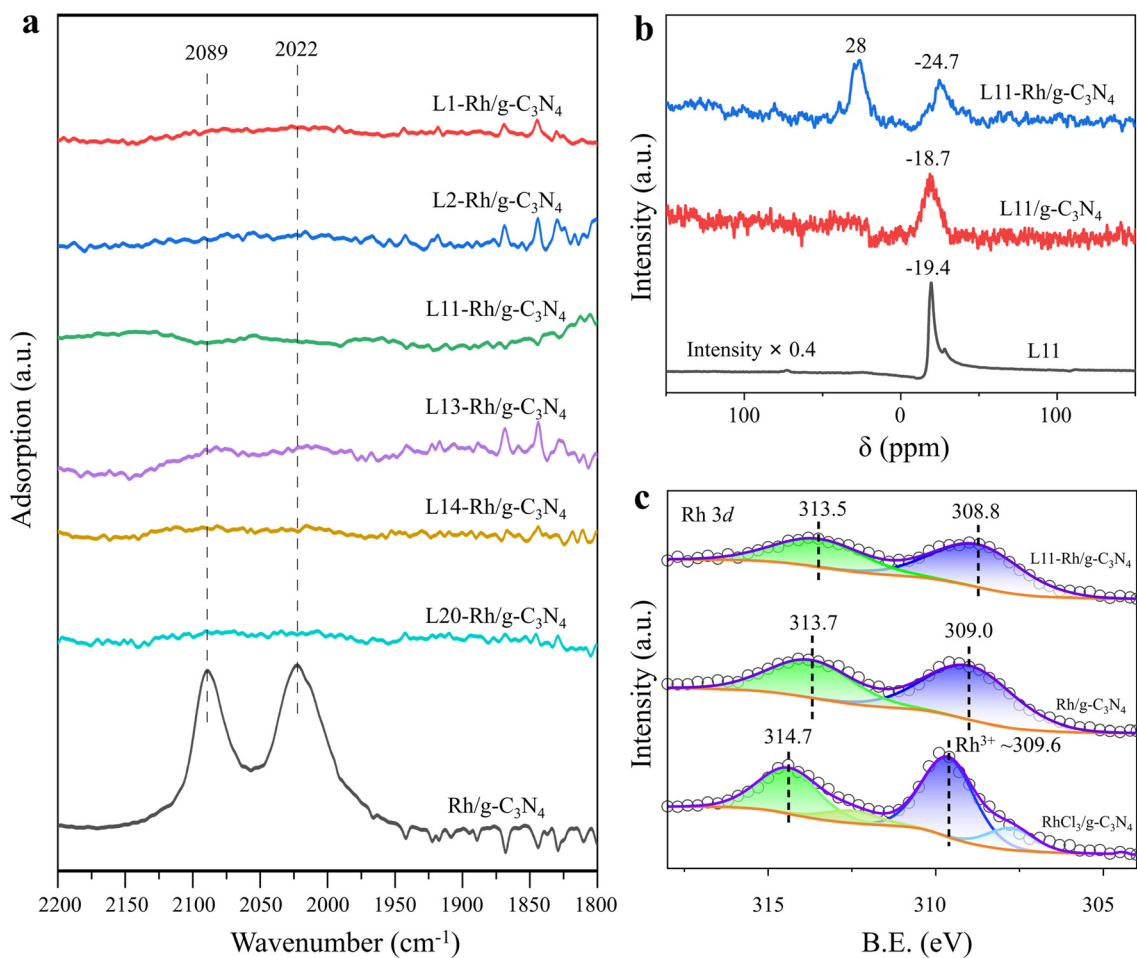

Fig. 2 (a) CO DRIFTS at 25 °C on Rh/g-C_3N_4 catalysts modified with representative ligands. All spectra were collected after CO adsorption (30 min) and Ar purging (1 h). (b) Solid-state ^{31}P MAS NMR spectra of L11–Rh/g-C_3N_4, L11/g-C_3N_4 (obtained by impregnating g-C_3N_4 with L11 under standard Schlenk conditions) and the pure L11 ligand. (c) XPS spectra of RhCl$_3$/g-C_3N_4 (obtained by impregnating g-C_3N_4 with RhCl$_3$·3H$_2$O and then directly dried without reduction), Rh/g-C_3N_4 and L11–Rh/g-C_3N_4.

148 | *Catal. Sci. Technol.*, 2025, **15**, 145–153

This journal is © The Royal Society of Chemistry 2025

suggesting the electron-donating effect of the ligand on Rh atoms.

Catalyst test on the hydroformylation of 1,3-butadiene to adipic aldehyde

The bimolecular hydroformylation of 1,3-butadiene to adipic aldehyde is a highly intricate reaction due to the presence of hydrogen gas in the system, facilitating facile hydrogenation. In addition to the target product adipic aldehyde (**1**), seven secondary products are predominantly formed: 1-cyclopenten-1-carbaldehyde (**2**), cyclopentanecarbaldehyde (**3**), 4-pentenal (**4**), 3-pentenal (**5**), 2-pentenal (**6**), valeraldehyde (**7**), and 2-methyl butyraldehyde (**8**), as depicted in Table 1. The support constitutes a significant distinction between heterogeneous and homogeneous catalysts. Initially, we investigated the influence of the support on the selectivity towards **1**. For Rh catalysts supported on alumina, some ligands commonly employed in homogeneous hydroformylation[8] were tested (Table 1, entries 1–7). Among them, Rh catalysts modified with DPPB, Xantphos and NiXantphos demonstrated selectivity to C_6 products (entries 5–7). However, only the condensation products **2** and **3** of adipic aldehyde (**1**) were observed, without the presence of **1** itself. We assumed that acidic sites on the surface of alumina could be responsible for the condensation of adipic aldehyde (**1**). Some other conventional supports, such as MCM-41 and silica gel, were also tested. However, the Rh loadings on these supports were low and no catalytic activity for adipic aldehyde was observed. Finally, g-C_3N_4 was selected as the main support due

to its neutral feature and several ligands were used to modify the catalysts, resulting in considerable selectivity towards **1** (entries 8–11 in Table 1). Preliminary investigations suggested that the ligand played a crucial role in the selectivity to C_6 products, especially for adipic aldehyde (**1**) (entry 12).

The impact of external factors such as reaction temperature and synthesis gas pressure on the reaction selectivity was then studied. With the increase in reaction temperature (Table 1 and S1†), the selectivity towards **1** gradually decreased, while the selectivity towards by-product **3** steadily increased, indicating that elevated temperature promoted the condensation of adipic aldehyde. Conversely, when the reaction temperature dropped to 80 °C, a reduction in selectivity towards **1** and by-product **7** was observed, accompanied by a relative increase in selectivity towards by-product **5**. This suggested that at lower temperature, both hydrogenation activity and second-molecule hydroformylation activity would decrease. The influence of gas pressure on the selectivity towards adipic aldehyde (**1**) is depicted in Table S2.† The selectivity towards **1** was highest at a pressure of 4 MPa (entry 4). Either lower or higher than 4 MPa could lead to formation of by-products **7** and **8** (entries 1–3 and 5), with a particularly pronounced increase observed at higher pressure (entry 5). This phenomenon may be attributed to the competitive nature of hydroformylation and hydrogenation reactions, with hydroformylation reaching an optimal ratio at 4 MPa.

According to the preliminary catalytic performance, the ligands played a key role in the selectivity of 1,3-butadiene hydroformylation. Based on the electron-donating ability and

---

Table 1 Screening of catalysts for the catalytic hydroformylation of 1,3-butadiene

Entry	Catalyst	Conv. (%)	Sel.[b] (%)								Carbon balance %
			1	2	3	4	5	6	7	8	
1[a]	RhCl$_3$/Al$_2$O$_3$	91.0	0	0	0	0	0	0	22.7	77.3	75.3
2[a]	Rh/Al$_2$O$_3$	99.5	0	0	0	2.2	11.1	0	18.0	68.7	76.4
3[a]	DPPM–Rh/Al$_2$O$_3$	100	0	0	0	0	0	0	45.0	55.0	80.6
4[a]	DPPE–Rh/Al$_2$O$_3$	99.7	0	0	0	3.4	13.4	0	30.1	53.1	82.2
5[a]	DPPB–Rh/Al$_2$O$_3$	87.3	0	1.1	21.4	6.5	0	0	70.0	1.0	88.5
6[a]	Xantphos–Rh/Al$_2$O$_3$	99.4	0	0	0.4	3.2	11.1	0	28.1	57.2	86.0
7[a]	NiXantphos–Rh/Al$_2$O$_3$	98.6	0	0.2	8.9	4.3	5.0	0	43.6	38.0	87.3
8[a]	DPPB–Rh/g-C$_3$N$_4$	89.6	3.7	1.1	9.0	13.3	3.7	0	68.4	0.8	89.8
9[c]	DPPB–Rh/g-C$_3$N$_4$	89.6	4.8	0.1	3.4	5.6	22.1	14.5	49.1	0.4	91.2
10[c]	Xantphos–Rh/g-C$_3$N$_4$	85.8	4	0.8	0	7.1	39	22.2	25.2	1.7	92.6
11[c]	NiXantphos–Rh/g-C$_3$N$_4$	98.1	13.7	0.1	3	0.5	8.4	0	56.8	17.5	98.7
12[c]	Rh/g-C$_3$N$_4$	82.6	0	0	0	0	0	0	30.0	70.0	77.2

[a] Reaction conditions: 1 g 1,3-butadiene solution (7.81 wt% in toluene), 4 g toluene, 1 mol% Rh catalyst, 4 MPa CO/H$_2$ (1:1), 110 °C, 10 h. The loading of Rh in the catalysts was 1 wt% unless otherwise stated. [b] Selectivity to aldehyde products in the liquid phase. [c] Reaction conditions: 90 °C, 10 h.
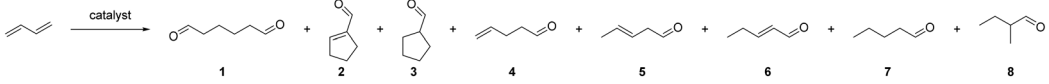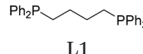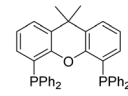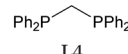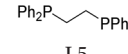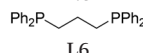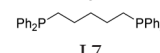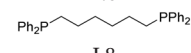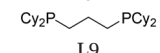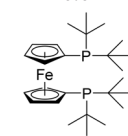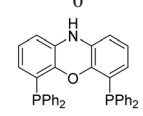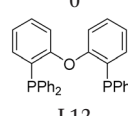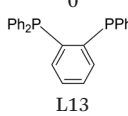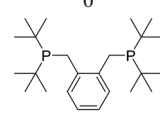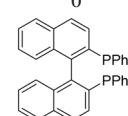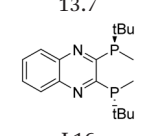
steric hindrance of the ligands, we comprehensively investigated the catalytic performance of the supported Rh atoms modified with different ligands. Initially, the commonly used ligands L1, L2 and L3 in homogeneous hydroformylation were tested,[8] where L1 and L3 exhibited selectivity towards **1**. Subsequently, a series of ligands accessible to us were screened for the 1,3-butadiene hydroformylation, including ligands analogous to L1 (L4–L9), L2 (L10), and L3 (L11, L12, L19), and also some other structures (Table 2). Among the 20 ligands tested, half displayed selectivity towards **1**, and 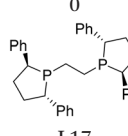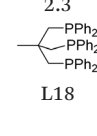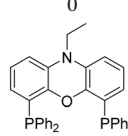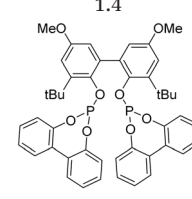L11 modified Rh atoms (L11–Rh/g-C$_3$N$_4$) demonstrated the highest selectivity of 13.7%. L11–Rh/g-C$_3$N$_4$ exhibited the highest selectivity towards adipic aldehyde (**1**), which can be explained from two perspectives: steric hindrance and electronic effects. From the perspective of steric hindrance, it is potentially attributed to the appropriate ligand bite angle of L11.[34,35] Regarding electronic effects, the substitution of the H group on N with ethyl (L19) markedly decreased the selectivity to **1**, highlighting the crucial role of protons in the 1,3-butadiene hydroformylation.[36,37] Comprehensive data on the impact of ligands on reaction selectivity are provided in Table S3.†

For the g-C$_3$N$_4$ support, we have investigated the density effect of Rh on the support (Table S3† entries 11 and 14–16). We found that at a loading of 1 wt%, the selectivity to **1** was

13.7%. As the loading increased, the selectivity to **1** gradually decreased, while the selectivity for by-product **8** significantly increased. This phenomenon may be attributed to the aggregation of Rh atoms on the surface of the support, forming nanoparticles (Fig. S2, S3c and d†). The recyclability of the catalyst was also tested, and a high selectivity to **1** could still be maintained after one cycle of catalyst recycling (Table S3† entry 12). In the second recycling, a notable decrease in the selectivity to **1** was observed (Table S3† entry 13), due to the leaching of Rh during the reaction process. ICP-OES revealed that after two cycles, the Rh loading turned to be from 1 wt% to 0.49 wt%. The HAADF-STEM image of the catalyst after two cycles indicated that there was no aggregation of Rh atoms after recycling (Fig. S3a and b†).

Fig. 3 illustrates the trends in the conversion of 1,3-butadiene and the selectivity towards C$_6$ products (**1**, **2**, and **3**) during the reaction time. Within the range of 0–600 minutes, the conversion of 1,3-butadiene rapidly increased to over 97%. The selectivity towards adipic aldehyde steadily increased, reaching a maximum value of 13.7% at 600 minutes. The selectivity towards the condensation product **3** initially rose rapidly to 2.7% during the early stages of the reaction, and then maintained at around 2%. Beyond 600 minutes, there was a noticeable decrease in the selectivity

Table 2 Effect of the ligand on the hydroformylation of 1,3-butadiene[a]

Ligand					
	L1	L2	L3	L4	L5
Sel. of 1/%	4.8	0	4.0	0	0.6
Ligand	L6	L7	L8	L9	L10
Sel. of 1/%	0	0	0	0	0
Ligand	L11	L12	L13	L14	L15
Sel. of 1/%	13.7	0	2.3	0	1.4
Ligand	L16	L17	L18	L19	L20
Sel. of 1/%	2.0	0.6	0	4.2	8.3

[a] Reaction conditions: 1 g 1,3-butadiene solution (7.81 wt% in toluene), 4 g toluene, 1 mol% Ln–Rh/g-C$_3$N$_4$, 4 MPa CO/H$_2$ (1:1), 90 °C, 10 h.

150 | *Catal. Sci. Technol.*, 2025, **15**, 145–153

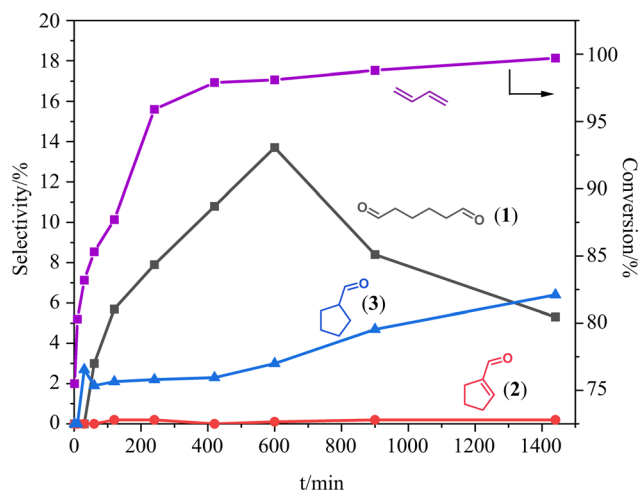This journal is © The Royal Society of Chemistry 2025

Fig. 3 Effect of reaction time on the hydroformylation of 1,3-butadiene by L11–Rh/g-C$_3$N$_4$. Reaction conditions: 3.5 g 1,3-butadiene solution (6.21 wt% in toluene), 12.5 g toluene, 1 mol% L11–Rh/g-C$_3$N$_4$, 4 MPa CO/H$_2$ (1 : 1), 90 °C.

towards **1**, accompanied by an increase in the selectivity towards **3**, indicating that prolonged reaction time can lead to the condensation of adipic aldehyde (**1**). The selectivity towards **2** remained consistently low, suggesting that it underwent hydrogenation immediately after the condensation of adipic aldehyde (**1**). To further confirm that the reaction occurred on the surface of the catalyst rather than in the solution, the catalyst was filtered off after 2 hours of reaction, and the filtrate was stirred for another 8 hours. However, the conversion of 1,3-butadiene remained unchanged, and the selectivity towards **1** did not increase but slightly decreased, possibly due to the condensation of **1**. Therefore, the reaction indeed occurred on the surface of the catalyst, rather than the Rh species leached from the support.

Research on the reaction mechanism

To investigate the catalytically active sites formed under reaction conditions and the role of the ligand in the reaction, we performed *in situ* CO DRIFTS on Rh/g-C$_3$N$_4$ and L11–Rh/g-C$_3$N$_4$ in the presence of CO and synthesis gas, as shown in Fig. 4. For Rh/g-C$_3$N$_4$, two distinct bands at 2086 cm^{-1} and 2020 cm^{-1} were observed under 0.5 MPa at 90 °C with exposure to CO, which was consistent with Fig. 2. After switching to a CO/H$_2$ atmosphere, there were no significant changes in either the intensity or position of the bands, indicating that the adsorption mode of CO on Rh remained unchanged (Fig. 4a). For L11–Rh/g-C$_3$N$_4$, two distinct bands at 2084 cm^{-1} and 2006 cm^{-1} were observed with exposure to CO, suggesting that increased pressure facilitates the adsorption of CO on the catalyst surface (Fig. 4b). These two peaks exhibited slight shifts compared to those in Fig. 4a, possibly due to the influence of the L11 ligand. After switching to CO/H$_2$ reaction gas under 0.5 MPa at 90 °C, four distinct peaks appeared at 2082 cm^{-1}, 2008 cm^{-1}, 1985 cm^{-1}, and 1963 cm^{-1} with analogy to the homogeneous system, which corresponded to signals of CO under two different chelation modes of the ligand: bis-equatorial chelation and equatorial-axial chelation.[17,34] Therefore, supported Rh atoms with the phosphine ligand possibly shared a similar mechanism of hydroformylation of 1,3-butadiene to the homogeneous system.

Based on the activation of CO (Fig. 4) and reported work on homogeneous hydroformylation,[3] we proposed a possible reaction mechanism (Scheme 1). Firstly, under the reaction conditions, a trigonal bipyramidal intermediate similar to the homogeneous catalyst was formed on the surface of the catalyst, with an outer layer of Rh stabilized by 18 electrons. Desorption of CO from this intermediate yielded a 16-electron rhodium hydride. Subsequently, the rhodium hydride underwent an addition reaction with 1,3-butadiene, with two modes of
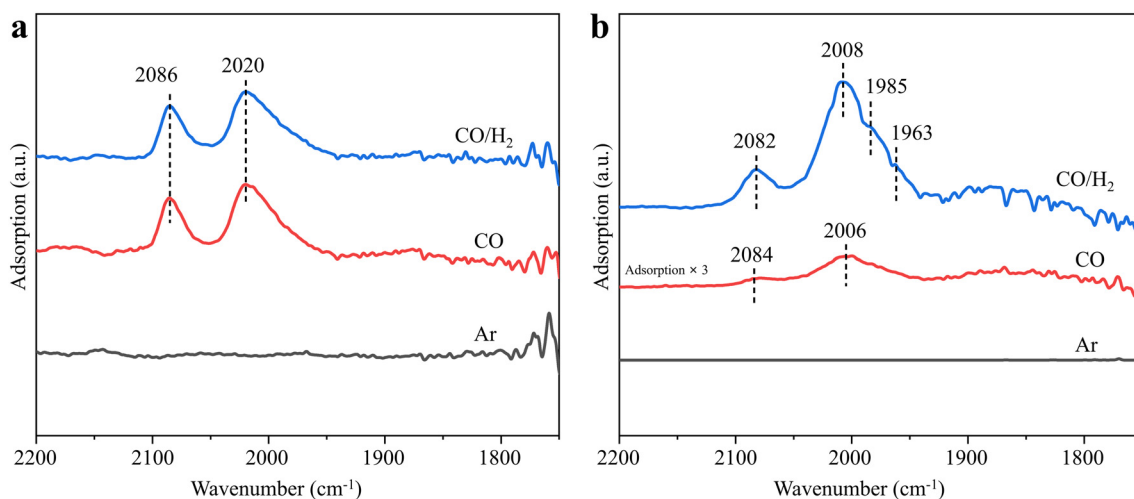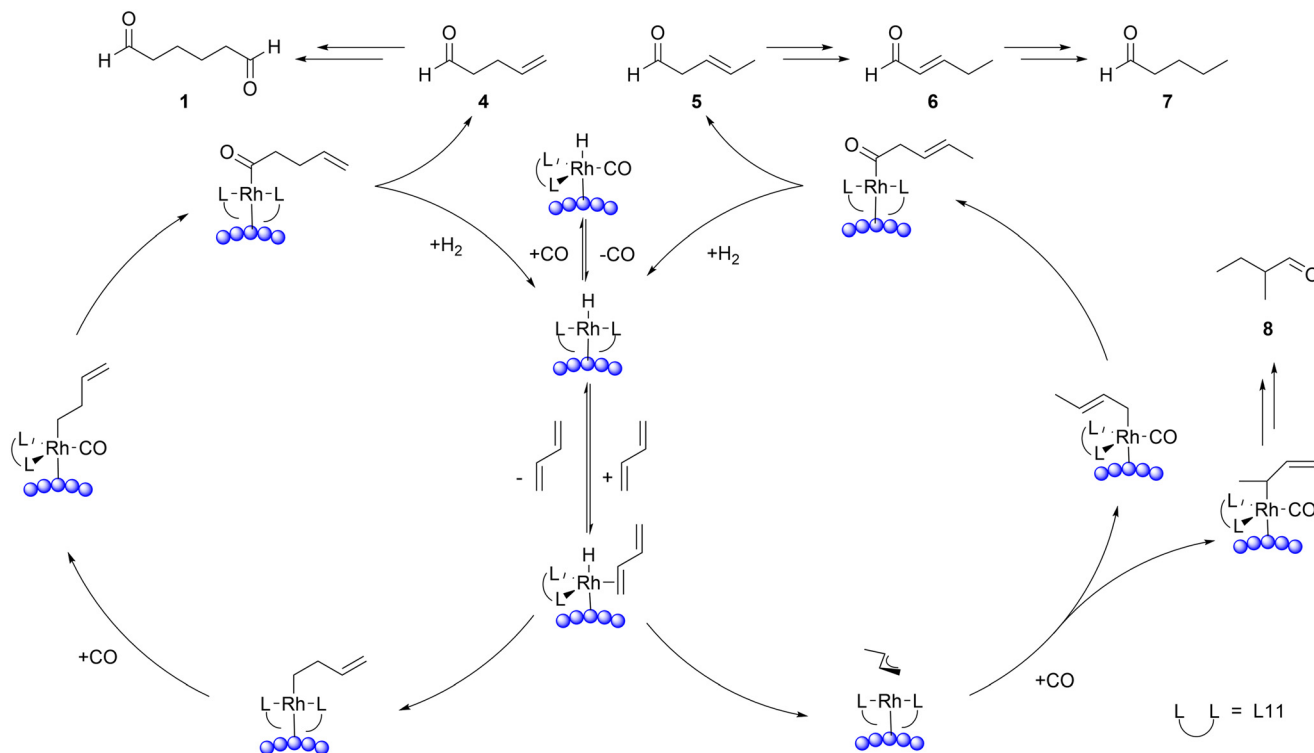

Fig. 4 *In situ* DRIFTS of gas adsorption at 90 °C on (a) Rh/g-C$_3$N$_4$ and (b) L11–Rh/g-C$_3$N$_4$ catalysts. All spectra were collected after gas adsorption (30 min) and Ar purging (1 h), and the gas pressure was 0.5 MPa.

This journal is © The Royal Society of Chemistry 2025

Catal. Sci. Technol., 2025, **15**, 145–153 | **151**

Scheme 1 Proposed mechanism for the hydroformylation of 1,3-butadiene. For trigonal-bipyramidal intermediates, only the bis-equatorial chelate coordination modes are displayed.

addition: normal addition and branched (iso) addition. Normal addition followed by insertion of a CO molecule yielded **4**, which underwent another round of hydroformylation to produce **1**. Branched addition followed by insertion of a CO molecule yielded **5**, which readily isomerized to **6**, subsequently undergoing rapid hydrogenation to form **7**. Product **8** was also derived from branched addition. By comparing the data presented in Fig. 4a and b, we observed that the ligand significantly weakens the interaction between CO and Rh atoms, thereby facilitating the dissociation and insertion of CO during the hydroformylation. Furthermore, the steric effects of the ligand promote normal addition. However, catalysts without ligands tend to favor iso-addition, resulting in the production of mono-hydroformylation products (Table 1, entries 1, 2 and 6).

Conclusions

In summary, we have developed ligand-modified Rh/g-C$_3$N$_4$ catalysts for the efficient hydroformylation of 1,3-butadiene to adipic aldehyde. HAADF-STEM, XRD, CO DRIFTS, ^{31}P MAS NMR and XPS confirm that Rh atoms are atomically dispersed on the g-C$_3$N$_4$ surface, with the ligand coordination and the electron-donating effect. Factors such as temperature, gas pressure, ligand structure, Rh loading, and reaction time all have significant effects on the selectivity towards adipic aldehyde. With L11 as the optimized ligand, the highest selectivity towards adipic aldehyde, at 13.7%, could be achieved at 90 °C and with 4 MPa synthesis gas for 10 hours. Using the g-C$_3$N$_4$ supported Rh atoms with phosphine ligand coordination,

we could achieve the heterogeneous hydroformylation of 1,3-butadiene to adipic aldehyde and get an insight into the activation of CO in the heterogeneous system, suggesting a similar mechanism of 1,3-butadiene hydroformylation compared to the homogeneous system.

Data availability

The data supporting this article have been included as part of the ESI.†

Author contributions

Huan Yan: supervision, conceptualization, funding acquisition, writing – review & editing. Lijin Gan: investigation, validation, data curation, writing – original draft. Zekun Liu, Lei Feng, Yi Duan, Guangyuan Xu and Si Chen: data discussion, writing – review & editing.

Conflicts of interest

There are no conflicts to declare.

Acknowledgements

References

1 H.-J. A. K. Weissermel, *Industrial Organic Chemistry*, Wiley-VCH, Weinheim, Germany, 4th edn, 2003.

2 R. Franke, D. Selent and A. Borner, *Chem. Rev.*, 2012, **112**, 5675–5732.

3 S. E. Smith, T. Rosendahl and P. Hofmann, *Organometallics*, 2011, **30**, 3643–3651.

4 S. Schmidt, P. Deglmann and P. Hofmann, *ACS Catal.*, 2014, **4**, 3593–3604.

5 S. Schmidt, E. Barath, C. Larcher, T. Rosendahl and P. Hofmann, *Organometallics*, 2015, **34**, 841–847.

6 T. Maji, C. H. Mendis, W. H. Thompson and J. A. Tunge, *J. Mol. Catal. A: Chem.*, 2016, **424**, 145–152.

7 M. J. Tenorio, R. V. Chaudhari and B. Subramaniam, *Ind. Eng. Chem. Res.*, 2019, **58**, 22526–22533.

8 S. M. Yu, W. K. Snavely, R. V. Chaudhari and B. Subramaniam, *Mol. Catal.*, 2020, **484**, 110721.

9 K. Zhao, X. Wang, D. He, H. Wang, B. Qian and F. Shi, *Catal. Sci. Technol.*, 2022, **12**, 4962–4982.

10 S. K. Sharma, P. A. Parikh and R. V. Jasra, *J. Mol. Catal. A: Chem.*, 2010, **316**, 153–162.

11 V. S. R. Ganga, A. A. Dabbawala, K. Munusamy, S. H. R. Abdi, R. I. Kureshy, N.-U. H. Khan and H. C. Bajaj, *Catal. Commun.*, 2016, **84**, 21–24.

12 E. Vunain, P. Ncube, K. Jalama and R. Meijboom, *J. Porous Mater.*, 2017, **25**, 303–320.

13 M. Tan, Y. Ishikuro, Y. Hosoi, N. Yamane, P. Ai, P. Zhang, G. Yang, M. Wu, R. Yang and N. Tsubaki, *Chem. Eng. J.*, 2017, **330**, 863–869.

14 H. J. Zhu, Y. J. Ding, L. Yan, J. M. Xiong, Y. Lu and L. W. Lin, *Catal. Today*, 2004, **93–95**, 389–393.

15 D. Han, X. Li, H. Zhang, Z. Liu, J. Li and C. Li, *J. Catal.*, 2006, **243**, 318–328.

16 D. Han, X. Li, H. Zhang, Z. Liu, G. Hu and C. Li, *J. Mol. Catal. A: Chem.*, 2008, **283**, 15–22.

17 S. Shylesh, D. Hanna, A. Mlinar, X.-Q. N. Kǒng, J. A. Reimer and A. T. Bell, *ACS Catal.*, 2013, **3**, 348–357.

18 Q. Sun, M. Jiang, Z. Shen, Y. Jin, S. Pan, L. Wang, X. Meng, W. Chen, Y. Ding, J. Li and F.-S. Xiao, *Chem. Commun.*, 2014, **50**, 11844–11847.

19 Q. Sun, Z. Dai, X. Liu, N. Sheng, F. Deng, X. Meng and F.-S. Xiao, *J. Am. Chem. Soc.*, 2015, **137**, 5204–5209.

20 C. Li, K. Sun, W. Wang, L. Yan, X. Sun, Y. Wang, K. Xiong, Z. Zhan, Z. Jiang and Y. Ding, *J. Catal.*, 2017, **353**, 123–132.

21 C. Li, W. Wang, L. Yan and Y. Ding, *Front. Chem. Sci. Eng.*, 2017, **12**, 113–123.

22 K. Dong, Q. Sun, Y. Tang, C. Shan, B. Aguila, S. Wang, X. Meng, S. Ma and F.-S. Xiao, *Nat. Commun.*, 2019, **10**, 3059.

23 X. Jia, Z. Liang, J. Chen, J. Lv, K. Zhang, M. Gao, L. Zong and C. Xie, *Org. Lett.*, 2019, **21**, 2147–2150.

24 T. Verheyen, N. Santillo, D. Marinelli, E. Petricci, W. M. De Borggraeve, L. Vaccaro and M. Smet, *ACS Appl. Polym. Mater.*, 2019, **1**, 1496–1504.

25 Z. Wang and Y. Yang, *RSC Adv.*, 2020, **10**, 29263–29267.

26 K. Zhao, H. Wang, X. Wang, T. Li, X. Dai, L. Zhang, X. Cui and F. Shi, *J. Catal.*, 2021, **401**, 321–330.

27 S. Ding, M. J. Hülsey, H. An, Q. He, H. Asakura, M. Gao, J.-Y. Hasegawa, T. Tanaka and N. Yan, *CCS Chem.*, 2021, **3**, 1814–1822.

28 Y. Zheng, Q. Wang, Q. Yang, S. Wang, M. J. Hulsey, S. Ding, S. Furukawa, M. Li, N. Yan and X. Ma, *ACS Catal.*, 2023, **13**, 7243–7255.

29 Z. Yu, S. Zhang, L. Zhang, X. Liu, Z. Jia, L. Li, N. Ta, A. Wang, W. Liu, A. Wang and T. Zhang, *J. Am. Chem. Soc.*, 2024, **146**, 11955–11967.

30 A. Wang, J. Li and T. Zhang, *Nat. Rev. Chem.*, 2018, **2**, 65–81.

31 F. Dong, L. Wu, Y. Sun, M. Fu, Z. Wu and S. C. Lee, *J. Mater. Chem.*, 2011, **21**, 15171–15174.

32 F. Dong, Z. Wang, Y. Sun, W.-K. Ho and H. Zhang, *J. Colloid Interface Sci.*, 2013, **401**, 70–79.

33 Y. Shi, X. Hu, J. Zhao, X. Zhou, B. Zhu, S. Zhang and W. Huang, *New J. Chem.*, 2015, **39**, 6642–6648.

34 L. A. van der Veen, P. H. Keeven, G. C. Schoemaker, J. N. H. Reek, P. C. J. Kamer, P. W. N. M. van Leeuwen, M. Lutz and A. L. Spek, *Organometallics*, 2000, **19**, 872–883.

35 T. Marimuthu, M. D. Bala and H. B. Friedrich, *Acta Crystallogr., Sect. E: Struct. Rep. Online*, 2008, **64**, o711.

36 H. Jiang, S. C. Sha, S. A. Jeong, B. C. Manor and P. J. Walsh, *Org. Lett.*, 2019, **21**, 1735–1739.

37 M. Y. S. Ibrahim and M. Abolhasani, *Nat. Commun.*, 2022, **13**, 2441.

This journal is © The Royal Society of Chemistry 2025

Catal. Sci. Technol., 2025, **15**, 145–153 | **153**